ARTICLE

# Tuning Thermal Transport in Ultrathin Silicon Membranes by Surface Nanoscale Engineering

**Sanghamitra Neogi,[*,†] J. Sebastian Reparaz,[‡] Luiz Felipe C. Pereira,[§] Bartlomiej Graczykowski,[‡] Markus R. Wagner,[‡] Marianna Sledzinska,[‡] Andrey Shchepetov,[⊥] Mika Prunnila,[⊥] Jouni Ahopelto,[⊥] Clivia M. Sotomayor-Torres,[‡,∥] and Davide Donadio[†]**

[†]Max Planck Institute for Polymer Research, Ackermannweg 10, 55128 Mainz, Germany, [‡]ICN2, Catalan Institute of Nanoscience and Nanotechnology, Campus UAB, 08193 Bellaterra, Barcelona, Spain, [§]Departamento de Fisica Teorica e Experimental, Universidade Federal do Rio Grande do Norte, Natal 59078-900, Brazil, [⊥]VTT Technical Research Centre of Finland, P.O. Box 1000, 02044 VTT, Espoo, Finland, and [∥]ICREA, Catalan Institute for Research and Advanced Studies, 08010 Barcelona, Spain

**ABSTRACT** A detailed understanding of the connections of fabrication and processing to structural and thermal properties of low-dimensional nanostructures is essential to design materials and devices for phononics, nanoscale thermal management, and thermoelectric applications. Silicon provides an ideal platform to study the relations between structure and heat transport since its thermal conductivity can be tuned over 2 orders of magnitude by nanostructuring. Combining realistic atomistic modeling and experiments, we unravel the origin of the thermal conductivity reduction in ultrathin suspended silicon membranes, down to a thickness of 4 nm. Heat transport is mostly controlled by surface scattering: rough layers of native oxide at surfaces limit the mean free path of thermal phonons below 100 nm. Removing the oxide layers by chemical processing allows us to tune the thermal conductivity over 1 order of magnitude. Our results guide materials design for future phononic applications, setting the length scale at which nanostructuring affects thermal phonons most effectively.

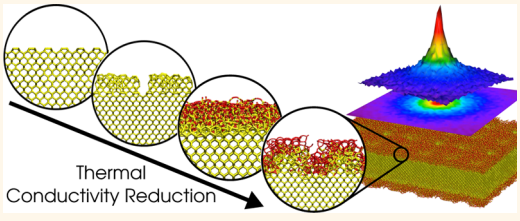


**KEYWORDS:** quasi-2D system · dispersion relations · Si membranes · lattice thermal transport · classical molecular dynamics · two-laser Raman thermometry · inelastic light scattering · phonon engineering

The emerging field of phononics has been fostering the development of materials and devices that can manipulate sound and heat with unprecedented precision. The main challenge is to enable harnessing heat transport in materials with the same degree of control already achieved for sound, by engineering the spectrum of THz phonons, which then requires designing materials at the nanoscale.[1,2] Phonon transport in nanostructures has indeed gained increasing attention in recent years[3−5] for thermal management at the nanoscale, efficient thermoelectric energy conversion, and in light of exploring new paradigms in information and communication technologies. Further developments in materials with tailored thermal transport properties stem from a detailed understanding of the behavior of phonons in low-dimensional and nanostructured systems.[3,6−12] In particular, major efforts have been devoted to reduce the thermal conductivity of silicon by nanostructuring, while preserving its electronic properties for thermoelectric applications.[8,13−19]

The thermal conductivity of silicon can be tuned over 2 orders of magnitude by engineering it at the nanoscale,[16] making it an ideal platform to study the relation between structure and heat transport. Advances in fabrication methods have made it possible to produce free-standing crystalline silicon membranes[20] with a thickness on the order of 10 nm, in which a reduction of the group velocities of phonons has been reported, leading to a reduction of over an order of magnitude in the in-plane thermal conductivity compared to bulk.[12,21] Mesoscopic models have been successfully used to develop a theory of thermal transport in silicon membranes,[22] in thin films,[23] and in silicon nanowires,[24] but there is evidence that such models based on bulk phonon properties

* Address correspondence to neogi@mpip-mainz.mpg.de.

Received for review November 28, 2014 and accepted March 31, 2015.

**Published online March 31, 2015**
**10.1021/nn506792d**

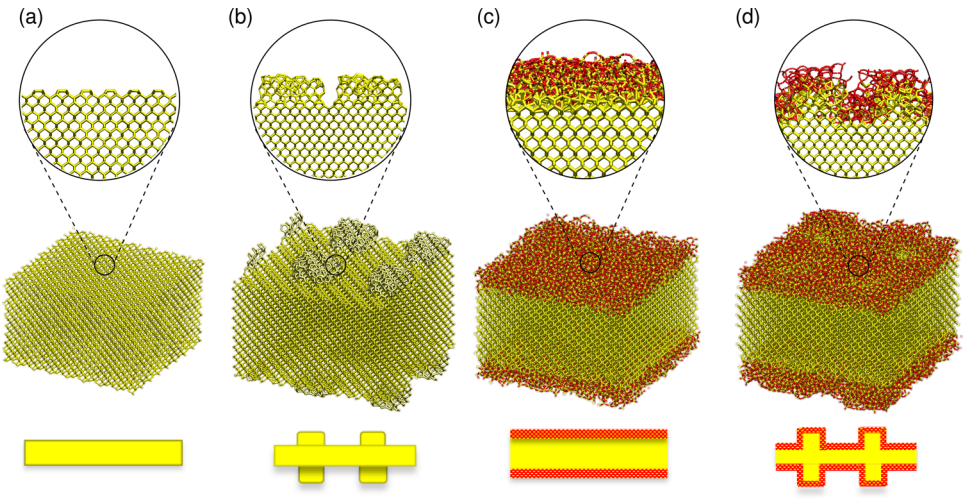


**Figure 1. Representative microscopic configurations of silicon membranes investigated in the present work: (a) crystalline silicon membrane with 2 × 1 reconstructed (001) surfaces, (b) rough silicon membrane with ∼1 nm high periodic surface features, (c) silicon membrane with a 1 nm thick layer of native oxide, and (d) silicon membrane with a rough native oxide at the top and bottom surfaces. Details about the preparation of the membrane configurations are given in the Methods section. Cartoons in the bottom row depict the corresponding configurations in the top row.**

would fail for both supported films and suspended membranes thinner than ∼20 nm.[25] Case in point: a compelling understanding of thermal transport in sub-20 nm thick membranes and of the microscopic origin of phonon surface scattering is lacking, as theoretical models incorporate surface effects through empirical specularity parameters or scattering functions, which do not establish any connection between surface structures and phonon transport.

Here we show that nanoscale surface features dictate heat transport in sub-20 nm thick silicon membranes, and we demonstrate experimentally how surfaces can be physically modified to tune at will the thermal conductivity. Our theoretical approach incorporates a complete microscopic description of the phonons in the membranes and does not rely on phenomenological assumptions on surface scattering. We demonstrate that dimensionality reduction significantly modifies the phonons in the membranes, which are strongly thickness-dependent and, hence, cannot be approximated with bulk phonon properties. We elucidate the interplay between several factors influencing thermal transport in the membranes by means of controlled experiments and modeling: thickness, the presence of surface native oxide layers, and surface roughness. We observe a large reduction of the in-plane thermal conductivity of ultrathin membranes with rough surface native oxide layers, up to ∼40 times smaller than bulk. We conclude that it is the presence of native oxide layers at the surface and to a lesser extent their roughness that mainly determine the thermal conductivity of sub-20 nm silicon membranes. Our results reveal that the main contribution to thermal conductivity comes from phonons with mean free paths shorter than 100 nm, thus suggesting that this is the length scale that should be targeted to further engineer these systems for phononic applications.

## RESULTS AND DISCUSSION

**Phonon Properties of the Membranes.** We investigated heat transport in free-standing single-crystalline silicon membranes with different nanoscale surface features consisting of varied surface roughness and native oxide layers. These suspended sub-10 nm thick silicon membranes were fabricated following the procedure outlined in ref 20. We measured the thickness of the membranes by pump-and-probe reflectivity measurements based on an asynchronous optical sampling method. The membrane thickness was determined from the frequency of the first-order dilatational mode (D1). We first performed measurements on the membranes with native oxide, which were eventually immersed in buffered HF to selectively etch the native oxide layers on both surfaces. The evidence of removal of the oxide layer was manifested by the change of the frequency of D1. Comparing the two measurements, we estimated the thickness of the native oxide layer to be 2.1 ± 0.1 nm, that is, ≈1 nm on each side of the free-standing silicon membranes. Supporting Information Figure S1 displays the reflectivity measurements of a 41 nm thick membrane with and without a native oxide layer.

Our atomistic models consist of single-crystalline silicon membranes oriented in the (001) direction, with thicknesses between 1 and 20 nm, with four different types of nanoscale surface features (Figure 1). We considered membranes with ideally reconstructed 2 × 1 surfaces (Figure 1a) and with rough surfaces (Figure 1b). Silicon membranes are exposed to atmospheric conditions during fabrication and measurements, which leads to the formation of a native oxide

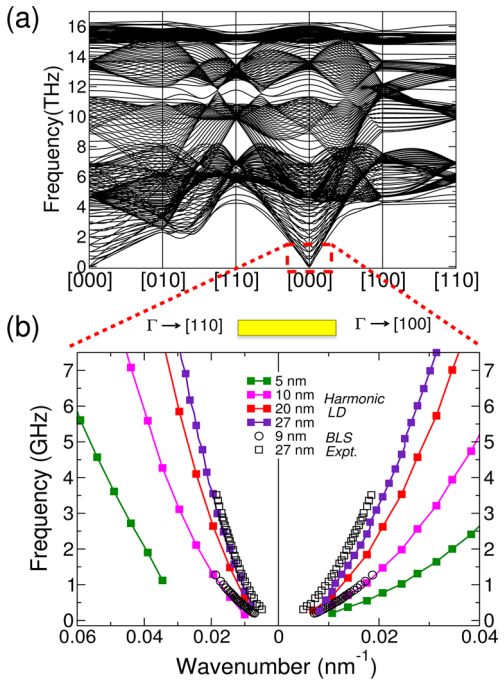


**Figure 2. Phonon dispersions in silicon membranes of different thicknesses: (a) dispersion in a 5 nm thick smooth membrane along different symmetry directions. The presence of flexural or breathing modes can be clearly noted in the figure. (b) Dispersion of flexural modes in silicon membranes at short wavevectors. The phase velocity of the modes increases with increasing thickness for both [100] and [110] symmetry directions. Theoretical results are represented with filled squares, and experimental data for 9 and 27 nm thick membranes are represented with black open circles and black open squares, respectively.**

layer of about 1−2 nm thickness on both surfaces, as measured in our experiments.[26] Since the roughness of the native oxide and silicon surface underneath can vary depending on the processing and storing conditions, we considered membrane models with 1 nm thick flat or rough silicon dioxide layers (Figure 1c,d). Interatomic interactions are modeled using empirical Tersoff potentials,[27,28] which reproduce well the thermal conductivities of both crystalline and amorphous silicon.[29,30] The atomistic models of membranes with rough surfaces, with or without native oxide, represent very closely the experimental samples.[31,32]

To assess the characteristics of phonons in free-standing silicon membranes compared to those in bulk, we measured the phonon dispersion relations by Brillouin light scattering (BLS) measurements and compared them to atomistic lattice dynamics calculations. The main effect of dimensionality reduction is the conversion of a transverse acoustic mode into an out-of-plane flexural mode (ZA), with quadratic dispersion at the zone center. Several higher-order flexural branches with finite frequencies appear at the Γ point, as shown in Figure 2a. The number of branches depends on the number of degrees of freedom in the unit cell and, therefore, increases with thickness. Due to the presence of flexural modes, the phonon dispersion relations of membranes are very different from those of the bulk, and for sub-10 nm systems, they cannot be approximated properly by zone folding of the bulk dispersion relations, which was mostly used in mesoscopic models.[22,25] The thickness of the membranes directly affects the dispersion of the out-of-plane ZA phonon modes at short wavevectors, which can be effectively probed by BLS.[12] Figure 2b, displaying a zoom on the dispersion relations of flexural modes at short wavevectors, shows that thinner membranes display softer ZA modes. The computed dispersion curve of the ZA branch of the 10 nm thick membrane (magenta-filled squares) agrees very well with the BLS measurement on an 8−10 nm thick membrane (black open circles). Similarly, good agreement between atomistic calculations (indigo-filled squares) and BLS experiments (black open squares) is found for the thickest membrane considered, 27 nm.[33] The results are especially consistent in the [110] symmetry direction. Remarkably, acoustic phonons at small wavevectors are not affected by surface features, as shown by a comparison between the dispersion relations of flat and rough silicon membranes in Supporting Information Figure S3. To the best of our knowledge, this is the first report of the direct connection of dimensionality reduction and surface roughness to phonon dispersion relations of silicon membranes, and we believe that the insight obtained here would be valuable for phononic crystal and acoustic metamaterial fabrication, in general.

On the whole, dimensionality reduction leads to flattening of the phonon dispersions, resulting in lower phonon group velocities with respect to the bulk. The thinner the membrane, the lower the phonon group velocities, leading to an expected reduction in thermal conductivity with decreasing thickness. Although surface roughness does not affect the acoustic phonon modes to a great extent, the dispersions of higher-frequency modes are flattened, leading to a further reduction of their group velocities. Surface roughness affects phonons with frequencies of about 1 THz and above, that is, in the range of the majority heat carriers of silicon,[25] thus hampering thermal transport.

**Thermal Conductivity of Ultrathin Membranes.** We measured the thermal conductivity of suspended silicon membranes by two-laser Raman thermometry (2LRT),[34] a novel technique developed to investigate the thermal transport properties of suspended membranes, and we computed the thermal conductivity of our atomistic model membranes from the fluctuations of the heat current in equilibrium molecular dynamics (EMD) simulations, following the Green−Kubo theory.[35] This approach accounts for anharmonic effects at all orders and does not rely on phenomenological assumptions on surface scattering. Both experiments and simulations refer to systems at room temperature. Our results are displayed in Figure 3, as a function of membrane

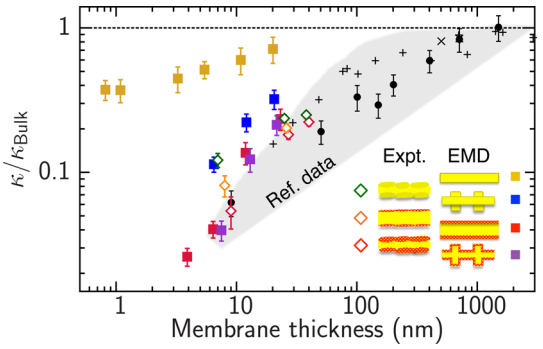


**Figure 3. Normalized computed and measured thermal conductivities ($\kappa/\kappa_{bulk}$) of silicon membranes at $T$ = 300 K as a function of membrane thickness. The filled squares represent results from EMD simulations computed using the Green−Kubo relation: yellow, blue, red, and violet squares represent smooth crystalline, rough crystalline, oxidized, and rough oxidized silicon membranes, respectively. The experimental data (open diamonds) are obtained using two-laser Raman thermometry. Red diamonds and green diamonds represent membranes with a native oxide layer and HF-etched membranes, respectively. The orange diamonds represent membranes with 6 h oxidation after etching. The black circles and the black pluses and crosses in the shaded area represent experimental data on silicon membranes[21,36] and SOI thin films,[37−40] respectively.**

thickness, and are compared to previous experiments on suspended membranes[21,36] and silicon thin films on insulators.[37−40] The thermal conductivities of membranes are normalized with respect to the bulk: for simulations, we use a bulk reference, $\kappa_{bulk}^{theo}$ = 197 ± 20 $Wm^{-1}$ $K^{-1}$,[29] and for experiments, $\kappa_{bulk}^{expt}$ = 148 $Wm^{-1}$ $K^{-1}$.[41]

Both computed and experimentally measured thermal conductivities grow as a function of thickness and asymptotically approach $\kappa_{bulk}^{theo}$ and $\kappa_{bulk}^{expt}$, respectively, for a thickness in the range of several hundreds of nanometers.[21,39] However, experiments show a significant reduction of $\kappa$ especially for the thinnest membranes (∼10 nm), while the computed $\kappa^{theo}$ of equivalently thin membranes with ideal 2 × 1 surface reconstruction is much less reduced. The ratio $\kappa^{theo}/\kappa_{bulk}^{theo}$ remains larger than 0.3 even for a 1 nm thick membrane model. $\kappa^{theo}/\kappa_{bulk}^{theo}$ for a 10 nm thick model is about 0.6, that is, approximately 10 times larger than that measured in this work (red diamond in Figure 3) and that reported in ref 21. This very large disagreement between theoretical and experimental observations indicates that dimensional reduction alone would not be sufficient to explain the thermal conductivity reduction to the extent observed in experiments. This case is analogous to that of silicon nanowires, which have relatively large thermal conductivity in their pristine crystalline form.[42−45] The computed thermal conductivities of membranes with native oxide (red and violet squares, respectively), however, are in much closer agreement with the experimental measurements. The normalized thermal conductivities of membranes with native oxide range from ∼0.025 to 0.25 for 4 and 22 nm thick models, respectively. Rough silica layers yield a lower $\kappa$ than flat ones within error bars. The effect of roughness is accentuated for the thickest membranes considered (10 and 20 nm), while it vanishes for the thinnest (∼7 nm), for which flat and rough oxidation leads to similar values of $\kappa^{theo}/\kappa_{bulk}^{theo}$. The maximum reduction of thermal conductivity is achieved for the ∼4 nm thick membranes with rough oxidized surfaces, which is 40 times less conductive than the bulk crystal. The reduction factor drops to 5 at 20 nm, implying that surface scattering is less significant for thicker membranes. In this perspective, the main effect of dimensional reduction is to provide systems with a very large surface-to-volume ratio, so that surface effects are greatly enhanced.

To disentangle the effects of oxidation and roughness, we simulated pure silicon membranes with rough surfaces. Rough surfaces are characterized by ∼1 nm high periodic features with a correlation length of about 2 nm, which is consistent with the roughness of experimental samples.[31,32] The surface nanostructuring of the rough membrane in Figure 3b is similar to that discussed in ref 46. We observe that surface roughness alone has a significant effect on the thermal conductivity (blue squares in Figure 3), although the reduction of $\kappa^{theo}$ is more limited than for membranes with native oxide. We indeed obtain a 9-fold reduction of $\kappa^{theo}$ for the 7 nm thick membrane, much smaller than the 25-fold reduction observed for that with native oxide. For thicker membranes, however, the difference becomes smaller; for example, for the rough 20 nm membrane, we computed a 3.1 reduction of $\kappa^{theo}$ compared to 4.6 obtained for that with rough native oxide. This picture is confirmed experimentally by comparing the thermal conductivities of silicon membranes with thicknesses of 9, 27, and 41 nm, before and after etching in buffered HF. Figure 4a displays the representative temperature decays in the 9 and 27 nm thick membranes with native oxide as measured using 2LRT.[34] The temperature decay in Figure 4b is a logarithm function of the distance from the center. The spatial dependence of the temperature field in two dimensions can be expressed as follows:[34]

$$T(r) = T_0 - \frac{P_{abs}}{2\pi d\kappa}\ln(r/r_0) \quad (1)$$

where $P_{abs}$ is the power absorbed by the membrane, $d$ is its thickness, $\kappa$ is the thermal conductivity, and $(T_0; r_0)$ is a reference point in the temperature field. Thus, the slope of the temperature decay can be simply written as, $dT(r)/d\ln(r) = P_{abs}/(2\pi d\kappa)$ and is used to obtain the thermal conductivity of the membrane. The uncertainties in the experimental thermal conductivities are computed according to ref 34 and explained in the Methods section. In order to compare the thermal decays of the membrane before, after etching, and the reoxidation process, the thickness of the membrane as well as the absorbed power needed to be

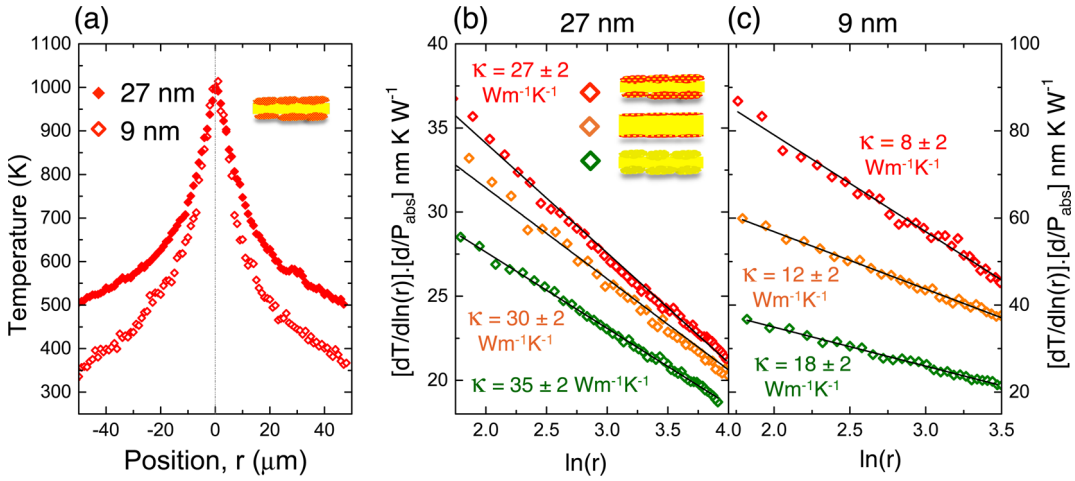


**Figure 4. Temperature decay profiles and thermal conductivity of silicon membranes with 9 and 27 nm in thickness with varied levels of native $SiO_2$ at the surfaces. (a) Thermal decays obtained using two-laser Raman thermometry.[34] Temperature decay in logarithmic scale for (b) 27 nm and (c) 9 nm membranes. The red, green, and orange diamonds represent membranes with native oxide, with oxide removed, and with 6 h of oxidation after etching, respectively; ln(*r*) is the logarithm of the distance *r* from the center.**

taken into account. Etching leads to a decrease in the membrane thickness by ~2 nm, and the reoxidation results in an increase by ~1 nm. Figure 4b displays the temperature decays in the 27 nm thick membrane with native oxide, after native oxide removal, as well as the decay in the etched membrane after 6 h of reoxidation. The membrane with native oxide has a thermal conductivity of 27 ± 2 $Wm^{-1}$ $K^{-1}$, while the thermal conductivity increases to 35 ± 2 $Wm^{-1}$ $K^{-1}$ after etching the native oxide layer. The reoxidation leads to a slight decrease in the thermal conductivity to 30 ± 2 $Wm^{-1}$ $K^{-1}$. The effect of etching and reoxidation is much more pronounced in the case of the 9 nm thick membrane. The membrane with native oxide has a thermal conductivity of 8 ± 2 $Wm^{-1}$ $K^{-1}$, whereas the thermal conductivity increases by 2.3-fold to 18 ± 2 $Wm^{-1}$ $K^{-1}$ after etching the native oxide layer. However, the thermal conductivity decreases by about 0.6 to 12 ± 2 $Wm^{-1}$ $K^{-1}$ after a 6 h reoxidation process. We note that thermal conductivities in the reoxidized membranes are intermediate between the cases with and without native oxide since full native oxide formation is only achieved after about 1 week.[26] The impact of etching and reoxidation on the thermal conductivity becomes less significant with the increase of membrane thickness. The thermal conductivity of the 41 nm thick membrane with a native oxide layer is found to be 33 ± 2 $Wm^{-1}$ $K^{-1}$, in good agreement with previous observations.[21] Upon etching, the thermal conductivity increases only 1.1-fold to 37 ± 2 $Wm^{-1}$ $K^{-1}$.

A direct comparison with the theoretical calculations shows excellent agreement in the case of the 9 nm thick membrane with and without native oxide, as shown in Figure 3. We note that the measured thermal conductivity is slightly lower compared to the computed value of the 27 nm thick etched membrane, although within the uncertainties. Such difference probably stems from the different roughness of the etched membrane. A direct comparison is difficult to make because it is not possible to quantify the roughness of the etched membrane. Theoretical calculations are very sensitive to the surface roughness: considering a 22 nm thick rough oxidized membrane as a reference, EMD simulations predict a 3.5-fold increase in $\kappa^{theo}$ for a 20 nm thick smooth crystalline membrane and a 1.5-fold increase $\kappa^{theo}$ for a 21 nm thick rough membrane with 1 nm high surface features emulating the membrane after removal of the oxide layer. The experiments show an increase in the thermal conductivity after oxide removal that follows the trend established by the calculations for these two cases. A phenomenological model with a predefined specularity parameter for surface scattering would not capture such effects.

We also computed the temperature dependence of $\kappa^{theo}$ of our silicon membrane models by EMD. For ideally surface-reconstructed membranes, $\kappa^{theo}$ is proportional to 1/*T*, indicating that anharmonic phonon–phonon scattering is the main process that controls thermal transport in these systems. In contrast, systems with rough and/or oxidized surfaces display a much weaker dependence of $\kappa^{theo}$ *versus* temperature, thus supporting the evidence that surface scattering dictates $\kappa^{theo}$ in ultrathin silicon membranes (see Supporting Information Figure S4).

**Mean Free Paths of Thermal Phonons.** The weak temperature dependence of the thermal conductivities of oxidized and rough membranes implies that the main limiting factor of phonon mean free paths in these systems is surface scattering. The main channel for phonon scattering is provided by surface roughness and oxidation. To quantify this effect, we use nonequilibrium MD (NEMD) in the quasi-ballistic regime[47] to compute the thermal conductivity accumulation

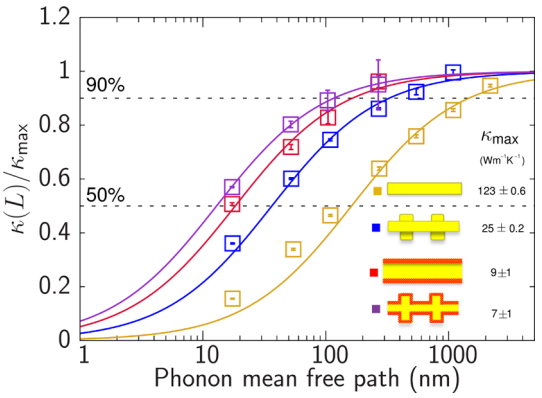


**Figure 5. Thermal conductivity accumulation functions in free-standing silicon membranes as a function of phonon mean free paths (MFP). The orange, blue, red, and violet squares represent a 5 nm thick smooth silicon membrane, a 7 nm thick nanopatterned crystalline membrane, a 7 nm thick oxidized membrane, and a 7 nm thick rough oxidized membranes, respectively. The solid lines are obtained utilizing the size dependence of thermal conductivities computed with the NEMD method, as explained in the text. The main effect of surface oxidation and roughness is to drastically shift the accumulation functions toward shorter MFPs. Fifty percent of thermal conductivity is contributed by phonons with MFPs up to ~160 nm in the smooth crystalline silicon membrane, while the same fraction is contributed by phonons with MFPs up to ~15 nm in the rough oxidized membrane. Ninety percent of the thermal conductivity in the rough crystalline membrane is contributed by phonons with MFPs shorter than ~100 nm.**

function, which provides an estimate of the contribution of phonons up to a given mean free path to the total thermal conductivity.[48,49]

In analogy with the former thermal spectroscopy experiments,[48] we performed NEMD simulations: the finite distance $L$ between the two thermal reservoirs kept at different temperatures determines a cutoff to the maximum mean free path of the phonons. Following the interpretation of these experiments,[48] we argue that the thermal conductivity $\kappa(L)$ of a finite system of length $L$ is the contribution to the total thermal conductivity of phonons with mean free path $\lambda < L$. Figure 5 shows the normalized accumulation functions of 5−7 nm thick silicon membranes with different surface nanoscale characters. We obtained the solid lines in Figure 5 utilizing the size dependence of $\kappa^{theo}(L)$:

$$\frac{1}{\kappa^{theo}(L)} = \frac{1}{\kappa_{max}} + \frac{\alpha}{L} \qquad (2)$$

where the normalization factor $\kappa_{max}$ is the asymptotic value of $\kappa^{theo}(L)$ as a function of $L$ for each atomistic membrane model and $\alpha$ is a fitting parameter. $\kappa_{max}$ represents the thermal conductivity of a macroscopic sample and corresponds to the $\kappa^{theo}$ value computed by EMD within error bars. We can define an average mean free path $\bar{\lambda}$ as the value of $\lambda$ for which the normalized $\kappa^{theo}(L)$ is $0.5\kappa_{max}$. There is no obvious linear correlation between the average mean free path $\bar{\lambda}$ and $\kappa^{theo}$, as noted in a former study[25] on supported silicon thin films. However, our accumulation function of 5 nm thick membrane (orange squares) with ideally reconstructed surface yields a $\bar{\lambda} \sim 160$ nm, while that of the bulk crystalline silicon from ref 49 is $\bar{\lambda} \sim 450$ nm. The ratio of the two $\bar{\lambda}$ values is ~2, which corresponds to the ratio $\kappa^{theo}/\kappa_{bulk}$, as shown in Figure 3. Furthermore, our 7 nm thick rough oxidized membrane (violet squares) has $\bar{\lambda} \sim 15$ nm, ~30-fold smaller than the bulk $\bar{\lambda}$, which is consistent with the reduction of $\kappa^{theo}$ in membranes with surface roughness. In any case, $\bar{\lambda}$ remains much larger than the membrane thickness (5−7 nm, in the cases considered here), indicating that there is no direct connection between the thickness of the membranes and the average phonon mean free paths; that is, the concept of the Casimir limit cannot be applied to ultrathin membranes to estimate the phonon mean free paths relevant for thermal transport.

The main effect of surface oxidation and roughness is to drastically shift the accumulation functions toward shorter $\lambda$, that is, to largely obstruct the propagation of phonons with long mean free paths and, consequently, their contribution to the thermal conductivity. Surface oxidation (red squares) and roughness (without oxidation, blue squares) lead to rather similar accumulation functions, while the combination of the two (violet squares) shifts the accumulation function toward even shorter phonon mean free paths. While the phonon mean free paths in the silicon membranes with ideally reconstructed surfaces remain fairly long (>1000 nm), phonons with mean free paths shorter than 100 nm contribute roughly 90% of the total thermal conductivity for the thinnest membrane with rough native oxide layers. This implies that phonons with mean free paths of ~100 nm dominate heat transport in rough oxidized silicon membranes, and further nanostructuring needs to be introduced at this length scale to engineer thermal transport in these systems.[15,19]

## CONCLUSIONS

Heat transport in ultrathin silicon membranes depends strongly upon the properties of the surface at the nanoscale, which is determined by processing and fabrication. By means of fabricating sub-10 nm free-standing single-crystal silicon membranes and direct measurements, we established the relationship between processing and thermal properties. We explained the interconnections between structural and thermal properties by realistic atomistic modeling of membranes with and without native oxide and different surface features. Our theoretical models provide thermal conductivity predictions in excellent agreement with experiments, without relying on phenomenological specularity scattering parameters or suppression functions, thereby unravelling the relationship between processing and structural and thermal properties of two-dimensional nanostructures.

We demonstrated that dimensional reduction directly affects the phonon dispersion relations by flattening the modes, especially the low-frequency out-of-plane acoustic modes in the membranes. The dimensional confinement modifies the phonon spectrum of the silicon membranes of all thicknesses; however, the modification alone does not hamper thermal transport to a great extent. In sub-10 nm thick silicon membranes, the main effect of dimensional reduction is to greatly enhance surface effects, and hence, surface scattering plays the dominant role. The presence of native oxide layers and the associated corrugation provide the main channel for phonon scattering to limit phonon mean free paths and are responsible for the dramatic reduction of thermal conductivity in ultrathin silicon membranes. Surface oxidation and roughness obstruct the propagation of phonons with long mean free paths and, consequently, limit the main contribution to the relatively small thermal conductivity of thin silicon membranes to phonons with mean free paths on the order of several tenths of nanometers. Heat transport in sub-10 nm silicon membranes is dictated by phonons with mean free paths shorter than 100 nm, which suggests that this is the length scale that should be targeted to further engineer these systems either for phononic applications in the THz regime or as thermal metamaterials. In turn, removing the oxide layer, such as by etching, restores a higher thermal conductivity, demonstrating that not only the roughness but also the chemical composition of the surface layers impacts thermal transport. Our study provides an insight and the tools to improve the phononic properties of nanostructured silicon, relevant for thermoelectric applications, as well as for the fabrication of phononic crystal and acoustic metamaterials.[50,51]

## METHODS

**Computational Details.** We computed the thermal conductivity of Si membranes from the fluctuations of the heat current in microcanonical molecular dynamics simulations, using the Green–Kubo relation:[35] $\kappa_\alpha = 1/(k_B V T^2)\int_0^\infty dt\langle J_\alpha(t)J_\alpha(0)\rangle$, where $\alpha = x, y$; $k_B$ is the Boltzmann constant, $V$ is the volume of the system, $T$ is the temperature, and $\langle J_\alpha(t)J_\alpha(0)\rangle$ is the heat current autocorrelation function along the direction ($\alpha$) of heat propagation. The heat current is given by $\mathbf{J} = \sum_i^N \varepsilon_i \mathbf{v}_i + {}^1/_2\sum_{i,j\neq j}^N (\mathbf{F}_{ij}\cdot\mathbf{v}_i)\mathbf{r}_{ij} + {}^1/_6\sum_{i,j,k;i\neq j\neq k}^N (\mathbf{F}_{ijk}\cdot\mathbf{v}_i)(\mathbf{r}_{ij}+\mathbf{r}_{ik})$, where $\varepsilon_i$ and $\mathbf{v}_i$ are the energy density and velocity associated with atom $i$, respectively. $\mathbf{F}$ represents the interatomic force acting between atoms separated by a distance $\mathbf{r}$. We applied periodic boundary conditions in the in-plane directions, thus mimicking the simulation of an infinite plane in the $x$ and the $y$ directions. The MD simulations were carried out using the LAMMPS package.[52] The equations of motion are integrated with a time step of 0.5 fs for systems containing only silicon and 0.25 fs for systems containing both silicon and oxygen to guarantee energy conservation over simulation times of several tens of nanoseconds. The interatomic forces were described using the empirical potential proposed by Tersoff,[27,28] which was parametrized to reproduce correctly the elastic properties of silicon and the structure of silicon/$SiO_2$ interfaces.

The smooth and nanopatterned crystalline membranes were constructed by replicating the unit cells of silicon membranes. The membrane unit cells of a certain thickness were prepared by cleaving bulk silicon along the (001) face. The (001) surface of silicon is the one used for technological applications, as it does not display metallic character, in contrast with the lower-energy (111) surface. The cleaved (001) surface undergoes a $2 \times 1$ reconstruction to minimize the number of dangling bonds, forming rows of dimers.[53] This reconstruction is energetically favorable and is stable beyond 900 K, which is the highest temperatures considered in this work. We prepared the rough silicon membrane configurations by cleaving nanopillars of $2 \times 2$ nm$^2$ area and 1 nm height from the silicon bulk at the two free membrane surfaces. The nanopillars are spaced about 2 nm apart. We heated the sample to 1500 K and then quenched it down to 300 K using a Langevin thermostat with an approximate cooling rate of $10^{11}$ K/s to obtain membranes with rough surfaces with ~1 nm high periodic features with a correlation length of ~2 nm. To generate the initial configuration of the models with native oxide, we introduced oxygen atoms at the surface of smooth crystalline silicon membranes and performed a cycle of annealing at 2000 K and quenching to room temperature with a rate of $10^{11}$ K/s using a Langevin thermostat.

In the EMD simulations to obtain thermal conductivities, the velocities were set to 300 K and the systems were again coupled to a Nosé–Hoover thermostat for 1 ns to decorrelate the systems from the initial configurations. The thermostat was then decoupled from the systems, and the heat flux calculations were performed under microcanonical conditions and recorded at 5 fs intervals. The total simulation time of the configurations varied between 20 and 30 ns. We have performed simulations with supercells of increasing $x$–$y$ dimensions to check for system size convergence and determined the dimension of our simulation supercell with minimum system size effects to have an area of $8.7 \times 8.7$ nm$^2$. Each of the $\kappa^{theo}$ values reported in Figure 3 was obtained averaging between 10 and 20 calculations performed with independent configurations, and the standard deviation is reported as the uncertainty.

In order to determine the thermal conductivity accumulation functions, we performed NEMD simulations by coupling the systems with two Langevin thermostats at 250 and 350 K, respectively, placing them at the two boundaries of the simulation cells along the $x$ direction. We recorded the temperature profile of the systems at approximate 1 nm interval along the $x$ direction to determine the thermal conductivities using Fourier's law: $\kappa = \lim_{t\to\infty} -\langle\langle J(t)\rangle\rangle/\langle\langle \partial T/\partial x\rangle\rangle$, where $J_x$ is the heat flux in the direction of transport under stationary conditions and $\langle\cdot\rangle$ indicates time averages. In general, NEMD methods require shorter simulation times when compared to the Green–Kubo method, but the simulation times are highly dependent on the system sizes and also depend on the system specifications. The total simulation times for our configurations varied between 20 and 60 ns, so that a stationary condition is achieved and a linear temperature profile is obtained. Block averaging of heat flux and temperature data were performed to obtain statistics on reported results.

**Experimental Details.** The free-standing single-crystal silicon membranes were fabricated using the method described in ref 20.

Brillouin light scattering measurements were performed using a six-pass tandem-type Fabry–Perot interferometer (JRS Scientific Instruments) at room temperature and in a (p-p) backscattering geometry (see inset of Supporting Information Figure S2).[33] The incident light with a wavelength of $\lambda_0 = 514.5$ nm ($Ar^+$ laser) was focused by using an Olympus 10× long working distance microscope objective. The laser spot had a diameter of approximately several micrometers, the incident power was kept below 1 mW, and the acquisition time was set to 15 min. Here, similarly to the case of surface Brillouin light scattering in opaque and semitransparent materials and due to

a small scattering volume, the dominant component of the inelastically scattered light comes from the surface ripple mechanism. Therefore, the momentum conservation is satisfied only for the in-plane components and the magnitude of the scattering wavevector $q$:[54]

$$q = \frac{4\pi \sin\theta}{\lambda_0} \quad (3)$$

where $\theta$ is the incident and scattered light angle. A representative spectrum of the 9 nm thick silicon membrane is shown in Supporting Information Figure S2.

Thermal conductivity measurements were conducted using two-laser Raman thermometry, a novel technique recently developed to investigate the thermal properties of suspended membranes.[34] A heating laser of $\lambda = 405$ nm was focused on the membranes using a microscope objective with NA = 0.55 in order to create a temperature gradient. The heating power was set to about 1 mW. The absorption coefficient of the 41 and 9 nm membranes was 25 and 7%, respectively. The probe laser was set to 488 nm, and its power was kept below 200 $\mu$W to avoid local heating while measuring the temperature field. The membranes with native $SiO_2$ were loaded into a cryostat which was evacuated to $10^{-4}$ mbar before the temperature decay measurements. In the second step, we chemically etched the native oxide layer at the surface and immediately reloaded the membranes into the cryostat to repeat the measurements under the same pressure conditions. Finally, we opened the cryostat to expose the membranes to air and let them oxidize for 6 h before repeating the measurements to obtain the thermal conductivities of membranes with an intermediate native oxide layer. The uncertainties in the measurements were assessed through error propagation of the equation determining the thermal conductivity of the membranes (eq 1): $\kappa$ = power/($2\pi d[dT/d\ln(r)]$), where "power" is the power absorbed by the membrane, $d$ is its thickness, and $\kappa$ is the thermal conductivity.[34] The relative error is obtained as $\Delta\kappa/\kappa = [|\Delta\text{power/power}|^2 + |\Delta d/d|^2 + |\Delta(dT/d\ln(r))/(dT/d\ln(r))|^2]^{1/2}$. The errors in the independent variables are $\Delta$power/power = 2%, $\Delta d/d$ = 1 nm/$d$, and the error in slope $\Delta(dT/d\ln(r))$ is obtained from fitting the data points as shown in Figure 4b,c.

*Conflict of Interest:* The authors declare no competing financial interest.

*Acknowledgment.* We thank Tristan Bereau and Kurt Kremer for critical reading of the manuscript. This work is partly funded by the European Commission FP7-ENERGY-FET project MERGING, NMP QUANTIHEAT and ICT NANOTHERM, with Grant Agreement Nrs: 309150, 604668 and 318117, respectively. S.N. and D.D. acknowledge financial support from MPG under the MPRG program. J.S.R., M.R.W., and C.M.S.T. acknowledge support form the Spanish MINECO projects TAPHOR (MAT-2012-31392) and nanoTHERM (CONSOLIDER CSD2010-00044). M.R.W. acknowledges support of the Marie Curie Postdoctoral Fellowship HeatProNano (Grant No. 628197). M.P. and A.S. acknowledge funding from the Academy of Finland (Grant No. 252598). S.N. and D.D. acknowledge the provision of computational facilities and support by Rechenzentrum Garching of Max Planck Society (MPG).

*Supporting Information Available:* Additional information and figures of the thickness measurements of the silicon membranes and computations of phonon dispersions and of temperature dependence of thermal conductivity of membranes. This material is available free of charge *via* the Internet at http://pubs.acs.org.

## REFERENCES AND NOTES

1. Li, N.; Ren, J.; Wang, L.; Zhang, G.; Hänggi, P.; Li, B. Colloquium: Phononics: Manipulating Heat Flow with Electronic Analogs and Beyond. *Rev. Mod. Phys.* **2012**, *84*, 1045.
2. Balandin, A. A.; Nika, D. L. Phononics in Low-Dimensional Materials. *Mater. Today* **2012**, *15*, 266–275.
3. Balandin, A. A. Nanophononics: Phonon Engineering in Nanostructures and Nanodevices. *J. Nanosci. Nanotechnol.* **2005**, *5*, 1015–1022.
4. Pop, E. Energy Dissipation and Transport in Nanoscale Devices. *Nano Res.* **2010**, *3*, 147–169.
5. Cahill, D. G.; Braun, P. V.; Chen, G.; Clarke, D. R.; Fan, S.; Goodson, K. E.; Keblinski, P.; King, W. P.; Mahan, G. D.; Majumdar, A. Nanoscale Thermal Transport. II. 2003−2012. *Appl. Phys. Rev.* **2014**, *1*, 011305.
6. Balandin, A.; Wang, K. L. Significant Decrease of the Lattice Thermal Conductivity Due to Phonon Confinement in a Free-Standing Semiconductor Quantum Well. *Phys. Rev. B* **1998**, *58*, 1544.
7. Chen, G. Phonon Heat Conduction in Nanostructures. *Int. J. Therm. Sci.* **2000**, *39*, 471–480.
8. Dresselhaus, M. S.; Chen, G.; Tang, M. Y.; Yang, R.; Lee, H.; Wang, D.; Ren, Z.; Fleurial, J.-P.; Gogna, P. New Directions for Low-Dimensional Thermoelectric Materials. *Adv. Mater.* **2007**, *19*, 1043–1053.
9. Chen, G.; Narayanaswamy, A.; Dames, C. Engineering Nanoscale Phonon and Photon Transport for Direct Energy Conversion. *Superlattices Microstruct.* **2004**, *35*, 161–172.
10. Vineis, C. J.; Shakouri, A.; Majumdar, A.; Kanatzidis, M. G. Nanostructured Thermoelectrics: Big Efficiency Gains from Small Features. *Adv. Mater.* **2010**, *22*, 3970–3980.
11. Li, J.-F.; Liu, W.-S.; Zhao, L.-D.; Zhou, M. High-Performance Nanostructured Thermoelectric Materials. *NPG Asia Mater.* **2010**, *2*, 152–158.
12. Cuffe, J.; Chávez, E.; Shchepetov, A.; Chapuis, P.-O.; El Boudouti, E. H.; Alzina, F.; Kehoe, T.; Gomis-Bresco, J.; Dudek, D.; Pennec, Y.; et al. Phonons in Slow Motion: Dispersion Relations in Ultrathin Si Membranes. *Nano Lett.* **2012**, *12*, 3569–3573.
13. Balandin, A. Thermal Properties of Semiconductor Low-Dimensional Structures. *Phys. Low-Dimens. Semicond. Struct.* **2000**, *1*−*2*, 1–28.
14. Lee, J.-H.; Galli, G. A.; Grossman, J. C. Nanoporous Si as an Efficient Thermoelectric Material. *Nano Lett.* **2008**, *8*, 3750–3754.
15. Yu, J.-K.; Mitrovic, S.; Tham, D.; Varghese, J.; Heath, J. R. Reduction of Thermal Conductivity in Phononic Nanomesh Structures. *Nat. Nanotechnol.* **2010**, *5*, 718–721.
16. Boukai, A. I.; Bunimovich, Y.; Tahir-Kheli, J.; Yu, J.-K.; Goddard, W. A.; Heath, J. R. Silicon Nanowires as Efficient Thermoelectric Materials. *Nature* **2008**, *451*, 168–171.
17. Toberer, E. S.; Baranowski, L. L.; Dames, C. Advances in Thermal Conductivity. *Annu. Rev. Mater. Res.* **2012**, *42*, 179–209.
18. Ikeda, H.; Salleh, F. Influence of Heavy Doping on Seebeck Coefficient in Silicon-on-Insulator. *Appl. Phys. Lett.* **2010**, *96*, 012106.
19. Tang, J.; Wang, H.-T.; Lee, D. H.; Fardy, M.; Huo, Z.; Russell, T. P.; Yang, P. Holey Silicon as an Efficient Thermoelectric Material. *Nano Lett.* **2010**, *10*, 4279–4283.
20. Shchepetov, A.; Prunnila, M.; Alzina, F.; Schneider, L.; Cuffe, J.; Jiang, H.; Kauppinen, E. I.; Sotomayor Torres, C. M.; Ahopelto, J. Ultra-thin Free-Standing Single Crystalline Silicon Membranes with Strain Control. *Appl. Phys. Lett.* **2013**, *102*, 192108.
21. Chávez-Ángel, E.; Reparaz, J.; Gomis-Bresco, J.; Wagner, M.; Cuffe, J.; Graczykowski, B.; Shchepetov, A.; Jiang, H.; Prunnila, M.; Ahopelto, J.; et al. Reduction of the Thermal Conductivity in Free-Standing Silicon Nano-membranes Investigated by Non-invasive Raman Thermometry. *APL Mater.* **2014**, *2*, 012113.
22. Johnson, J. A.; Maznev, A. A.; Cuffe, J.; Eliason, J. K.; Minnich, A. J.; Kehoe, T.; Sotomayor Torres, C. M.; Chen, G.; Nelson, K. A. Direct Measurement of Room-Temperature Nondiffusive Thermal Transport over Micron Distances in a Silicon Membrane. *Phys. Rev. Lett.* **2013**, *110*, 025901.
23. Aksamija, Z.; Knezevic, I. Anisotropy and Boundary Scattering in the Lattice Thermal Conductivity of Silicon Nanomembranes. *Phys. Rev. B* **2010**, *82*, 045319.
24. Martin, P.; Aksamija, Z.; Pop, E.; Ravaioli, U. Impact of Phonon-Surface Roughness Scattering on Thermal

Conductivity of Thin Si Nanowires. *Phys. Rev. Lett.* **2009**, *102*, 125503.
25. Turney, J. E.; McGaughey, A. J. H.; Amon, C. H. In-Plane Phonon Transport in Thin Films. *J. Appl. Phys.* **2010**, *107*, 024317.
26. Morita, M.; Ohmi, T.; Hasegawa, E.; Kawakami, M.; Ohwada, M. Growth of Native Oxide on a Silicon Surface. *J. Appl. Phys.* **1990**, *68*, 1272.
27. Tersoff, J. Modeling Solid-State Chemistry: Interatomic Potentials for Multicomponent Systems. *Phys. Rev. B* **1989**, *39*, 5566–5568.
28. Munetoh, S.; Motooka, T.; Moriguchi, K.; Shintani, A. Interatomic Potential for Si-O Systems Using Tersoff Parameterization. *Comput. Mater. Sci.* **2007**, *39*, 334–339.
29. He, Y.; Savić, I.; Donadio, D.; Galli, G. Lattice Thermal Conductivity of Semiconducting Bulk Materials: Atomistic Simulations. *Phys. Chem. Chem. Phys.* **2012**, *14*, 16209–16222.
30. He, Y.; Donadio, D.; Galli, G. Heat Transport in Amorphous Silicon: Interplay between Morphology and Disorder. *Appl. Phys. Lett.* **2011**, *98*, 144101.
31. Tong, Q.-Y.; Lee, T.-H.; Gösele, U.; Reiche, M.; Ramm, J.; Beck, E. The Role of Surface Chemistry in Bonding of Standard Silicon Wafers. *J. Electrochem. Soc.* **1997**, *144*, 384–389.
32. Feenstra, R.; Oehrlein, G. Surface Morphology of Oxidized and Ion-Etched Silicon by Scanning Tunneling Microscopy. *Appl. Phys. Lett.* **1985**, *47*, 97–99.
33. Graczykowski, B.; Gomis-Bresco, J.; Alzina, F.; Reparaz, J. S.; Shchepetov, A.; Prunnila, M.; Ahopelto, J.; Sotomayor Torres, C. Acoustic Phonon Propagation in Ultra-thin Si Membranes under Biaxial Stress Field. *New J. Phys.* **2014**, *16*, 073024.
34. Reparaz, J.; Chavez-Angel, E.; Wagner, M.; Graczykowski, B.; Gomis-Bresco, J.; Alzina, F.; Sotomayor Torres, C. M. A Novel Contactless Technique for Thermal Field Mapping and Thermal Conductivity Determination: Two-Laser Raman Thermometry. *Rev. Sci. Instrum.* **2014**, *85*, 034901.
35. Zwanzig, R. Time-Correlation Functions and Transport Coefficients in Statistical Mechanics. *Annu. Rev. Phys. Chem.* **1965**, *16*, 67–102.
36. Liu, X.; Wu, X.; Ren, T. *In Situ* and Noncontact Measurement of Silicon Membrane Thermal Conductivity. *Appl. Phys. Lett.* **2011**, *98*, 174104.
37. Asheghi, M.; Leung, Y.; Wong, S.; Goodson, K. Phonon-Boundary Scattering in Thin Silicon Layers. *Appl. Phys. Lett.* **1997**, *71*, 1798–1800.
38. Asheghi, M.; Touzelbaev, M.; Goodson, K.; Leung, Y.; Wong, S. Temperature-Dependent Thermal Conductivity of Single-Crystal Silicon Layers in SOI Substrates. *J. Heat Transfer* **1998**, *120*, 30–36.
39. Ju, Y.; Goodson, K. Phonon Scattering in Silicon Films with Thickness of Order 100 nm. *Appl. Phys. Lett.* **1999**, *74*, 3005–3007.
40. Liu, W.; Asheghi, M. Thermal Conduction in Ultrathin Pure and Doped Single-Crystal Silicon Layers at High Temperatures. *J. Appl. Phys.* **2005**, *98*, 123523.
41. Glassbrenner, C. J.; Slack, G. A. Thermal Conductivity of Silicon and Germanium from 3K to the Melting Point. *Phys. Rev.* **1964**, *134*, A1058–A1069.
42. Ponomareva, I.; Srivastava, D.; Menon, M. Thermal Conductivity in thin Silicon Nanowires: Phonon Confinement Effect. *Nano Lett.* **2007**, *7*, 1155–1159.
43. Donadio, D.; Galli, G. Atomistic Simulations of Heat Transport in Silicon Nanowires. *Phys. Rev. Lett.* **2009**, *102*, 195901.
44. He, Y.; Galli, G. Microscopic Origin of the Reduced Thermal Conductivity of Silicon Nanowires. *Phys. Rev. Lett.* **2012**, *108*, 215901.
45. Duchemin, I.; Donadio, D. Atomistic Simulations of Heat Transport in Real-Scale Silicon Nanowire Devices. *Appl. Phys. Lett.* **2012**, *100*, 223107.
46. Davis, B. L.; Hussein, M. I. Nanophononic Metamaterial: Thermal Conductivity Reduction by Local Resonance. *Phys. Rev. Lett.* **2014**, *112*, 055505.
47. Müller-Plathe, F. A Simple Nonequilibrium Molecular Dynamics Method for Calculating the Thermal Conductivity. *J. Chem. Phys.* **1997**, *106*, 6082–6085.
48. Minnich, A. J.; Johnson, J. A.; Schmidt, A. J.; Esfarjani, K.; Dresselhaus, M. S.; Nelson, K. A.; Chen, G. Thermal Conductivity Spectroscopy Technique To Measure Phonon Mean Free Paths. *Phys. Rev. Lett.* **2011**, *107*, 095901.
49. Regner, K. T.; Sellan, D. P.; Su, Z.; Amon, C. H.; Mcgaughey, A. J. H.; Malen, J. A. Broadband Phonon Mean Free Path Contributions to Thermal Conductivity Measured Using Frequency Domain Thermoreflectance. *Nat. Commun.* **2013**, *4*, 1640–7.
50. Alaie, S.; Su, M. F.; Goettler, D. F.; El-Kady, I.; Leseman, Z. Effects of Flexural and Extensional Excitation Modes on the Transmission Spectrum of Phononic Crystals Operating at Gigahertz Frequencies. *J. Appl. Phys.* **2013**, *113*, 103513.
51. Gorishnyy, T.; Ullal, C.; Maldovan, M.; Fytas, G.; Thomas, E. Hypersonic Phononic Crystals. *Phys. Rev. Lett.* **2005**, *94*, 115501.
52. Plimpton, S. Fast Parallel Algorithms for Short-Range Molecular Dynamics. *J. Comput. Phys.* **1995**, *117*, 1–19.
53. Appelbaum, J. A.; Baraff, G.; Hamann, D. The Si(100) Surface. III. Surface Reconstruction. *Phys. Rev. B* **1976**, *14*, 588.
54. Sandercock, J. R. *Light Scattering in Solids III*; Springer: Berlin, 1982; pp 173−206.